Crossover from interaction to driven regimes in quantum vortex reconnections

Luca Galantucci[a,1], Andrew W. Baggaley[a], Nick G. Parker[a], and Carlo F. Barenghi[a]

[a]Joint Quantum Centre Durham–Newcastle, School of Mathematics, Statistics and Physics, Newcastle University, Newcastle upon Tyne NE1 7RU, United Kingdom

Edited by Katepalli R. Sreenivasan, New York University, New York, NY, and approved May 6, 2019 (received for review October 31, 2018)

Reconnections of coherent filamentary structures play a key role in the dynamics of fluids, redistributing energy and helicity among the length scales, triggering dissipative effects, and inducing fine-scale mixing. Unlike ordinary (classical) fluids where vorticity is a continuous field, in superfluid helium and in atomic Bose–Einstein condensates (BECs) vorticity takes the form of isolated quantized vortex lines, which are conceptually easier to study. New experimental techniques now allow visualization of individual vortex reconnections in helium and condensates. It has long being suspected that reconnections obey universal laws, particularly a universal scaling with time of the minimum distance between vortices δ. Here we perform a comprehensive analysis of this scaling across a range of scenarios relevant to superfluid helium and trapped condensates, combining our own numerical simulations with the previous results in the literature. We reveal that the scaling exhibits two distinct fundamental regimes: a $\delta \sim t^{1/2}$ scaling arising from the mutual interaction of the reconnecting strands and a $\delta \sim t$ scaling when extrinsic factors drive the individual vortices.

reconnections | superfluid | quantum vortices | Bose–Einstein condensates

Reconnections of coherent filamentary structures (Fig. 1) play a fundamental role in the dynamics of plasmas (from astrophysics (1–3) to confined nuclear fusion), nematic liquid crystals (4), polymers and macromolecules (5) (including DNA (6)), optical beams (7, 8), ordinary (classical) fluids (9–11), and quantum fluids (12, 13). In fluids, the coherent structures consist of concentrated vorticity, whose character depends on the classical or quantum nature of the fluid: In classical fluids (air, water, etc.), vorticity is a continuous field and the interacting structures are vortex tubes of arbitrary core size around which the circulation of the velocity field is unconstrained; in quantum fluids (atomic Bose–Einstein Condensates [BECs] and superfluid ^{4}He and ^{3}He), the structures are isolated one-dimensional vortex lines, corresponding to topological defects of the governing order parameter around which the velocity's circulation is quantized (14–17).

The discrete nature of quantum vortices makes them ideal for the study of vortex reconnections, which assume the form of isolated, dramatic events, strongly localized in space and time. First conjectured by Feynman (15) and then numerically predicted (19), quantum vortex reconnections have been observed only recently, both in superfluid ^{4}He (20) (indirectly, using tracer particles) and in BECs (21) (directly, using an innovative stroboscopic visualization technique).

Vortex reconnections are crucial in redistributing the kinetic energy of turbulent superfluids. In some regimes, they trigger a turbulent energy cascade (22) in which vortex lines self-organize in bundles (23), generating the same Kolmogorov spectrum of classical turbulence (22, 24–27). By altering the topology of the flow (28), reconnections also seem to redistribute its helicity (29, 30), although the precise definition of helicity in superfluids is currently debated (30–32), and the effects of reconnections (33–36) on its geometric ingredients (link, writhe, and twist) are still discussed. In the low-temperature limit, losses due to viscosity or mutual friction are negligible, and reconnections are the ultimate mechanism for the dissipation of the incompressible kinetic energy of the superfluid via sound radiation at the reconnecting event (37, 38) followed by further sound emission by the Kelvin wave cascade (39–41) which follows the relaxation of the reconnection cusps.

Is There a Universal Route to Reconnection?

Many authors have focused on the possibility that there is a universal route to reconnection, which may take the form of a vortex ring cascade (42, 43), a particular rule for the cusp angles (44, 45), or, more promising, a special scaling with time of the minimum distance $\delta(t)$ between the reconnecting vortex strands. It is on the last property that we concentrate our attention.

Several studies have observed a symmetrical pre-/post-reconnection scaling of $\delta(t)$ (18, 44, 46–48); others have suggested an asymmetrical scaling possibly ascribed to acoustic energy losses (38, 49, 50), similar to the asymmetry observed in classical Navier–Stokes fluids (51). In Fig. 2, *Top* and *Bottom* we present a comprehensive summary of the scaling of $\delta(t)$, combining previous numerical and experimental results with data computed in the present study; this spans an impressive eight orders of magnitude.

The aim of this paper is to reveal that there are two distinct fundamental scaling regimes for $\delta(t)$. In addition to the known (18, 44, 46–48, 52–54) $\delta \sim t^{1/2}$ scaling, we predict and observe a new linear scaling $\delta(t) \sim t$. We show how the two scalings arise from rigorous dimensional arguments and then demonstrate them in numerical simulations of vortex reconnections.

Significance

Vortex reconnections are fundamental events in fluid motion, randomizing the velocity field, changing the topology, and redistributing energy across length scales. In superfluid helium and atomic Bose–Einstein condensates, vortices are effectively one-dimensional lines called quantum vortices (akin to minitornadoes of a fixed strength). Individual reconnections happen when two vortices collide and subsequently recoil, exchanging heads and tails. Recent experimental progress opens the possibility of answering the important question as to whether reconnections obey a universal behavior. Here we show that the intervortex distance between reconnecting vortices obeys two fundamental scaling laws, which we identify in experimental data and numerical simulations, across homogeneous superfluids and trapped condensates.

Author contributions: L.G., A.W.B., N.G.P., and C.F.B. designed research; L.G. and A.W.B. performed research; L.G. and A.W.B. contributed new reagents/analytic tools; L.G. analyzed data; and L.G., A.W.B., N.G.P., and C.F.B. wrote the paper.

The authors declare no conflict of interest.

This article is a PNAS Direct Submission.

[1]To whom correspondence may be addressed. Email: luca.galantucci@newcastle.ac.uk.

This article contains supporting information online at www.pnas.org/lookup/suppl/doi:10.1073/pnas.1818668116/-/DCSupplemental.

Published online June 6, 2019.

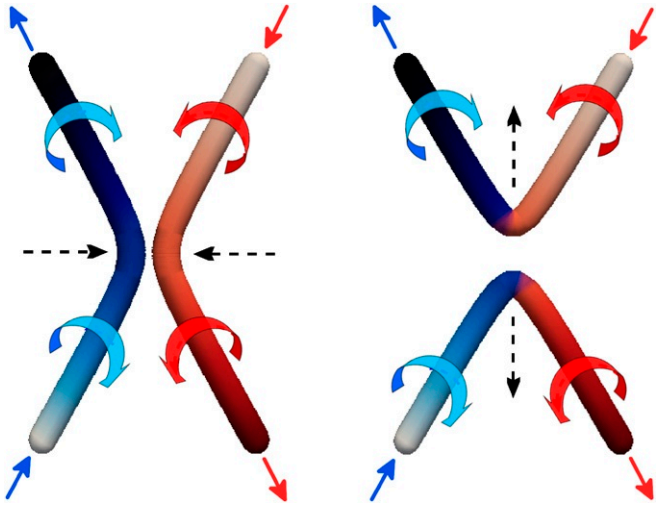

Fig. 1. Reconnecting vortex lines exchanging strands. Shown are schematic vortex configurations before the reconnection (*Left*) and after (*Right*); the vortices' shape is as determined analytically by Nazarenko and West (18). Color gradient along the vortices and blue/red arrows indicate the directions of the vorticity along the vortices and the direction of the flow velocity around them. Dashed black arrows indicate the vortex motion, first toward each other and then away from each other.

Dimensional Analysis

We conjecture that, in the system under consideration (superfluid helium, atomic BECs), δ depends only upon the following physical variables: the time t from the reconnection, the quantum of circulation κ of the superfluid, a characteristic length scale ℓ associated to the geometry of the vortex configuration, the fluid's density ρ, and the density gradient $\nabla\rho$. We hence postulate the following functional form:

$$f(\delta, t, \kappa, \ell, \rho, \nabla\rho) = 0. \quad [1]$$

Following the standard procedure of the Buckingham π-theorem (55) (see *SI Appendix*, section SI.1 for details), we derive the scalings

$$\delta(t) = (C_1\kappa)^{1/2} t^{1/2} \quad \textit{interaction regime}, \quad [2]$$

$$\delta(t) = C_2 \left(\frac{\kappa}{\ell}\right) t \quad \textit{driven regime}, \quad [3]$$

$$\delta(t) = C_3 \left(\kappa \frac{\nabla\rho}{\rho}\right) t \quad \textit{driven regime}, \quad [4]$$

where C_1, C_2, and C_3 are dimensionless constants. Physically, the $\delta \sim t^{1/2}$ scaling of Eq. **2** identifies the quantum of circulation κ as the only relevant parameter driving the reconnection dynamics (20); this scaling corresponds to vortex dynamics driven by the mutual interaction between vortex strands, as illustrated more in detail in *Homogeneous Unbounded Systems*.

Eqs. **3** and **4**, on the other hand, introduce the $\delta \sim t$ scaling. This scaling suggests the presence of a characteristic velocity which drives the approach/separation of the vortex lines. Indeed, we can offer some physical examples of these velocities. If ℓ is the radius of a vortex ring, then $v_\ell = C_2(\kappa/\ell)$ is, to a first approximation, the self-induced velocity of the ring. Alternatively, if ℓ is equal to the distance of a vortex to a sharp boundary in an otherwise homogeneous BEC (such as arises for BEC confined by box traps), then v_ℓ is the self-induced vortex velocity arising from the presence of an image vortex. Finally, if the BEC density is smoothly varying (such as arises for BECs confined by harmonic traps), then $v_{\nabla\rho} = C_3(\kappa\nabla\rho/\rho)$ is precisely the individual velocity of a vortex induced by the density gradients, with C_3 depending on the trap's geometry (56, 57). In the next section we will see how these scalings, and the crossover, emerge in typical scenarios through numerical simulations.

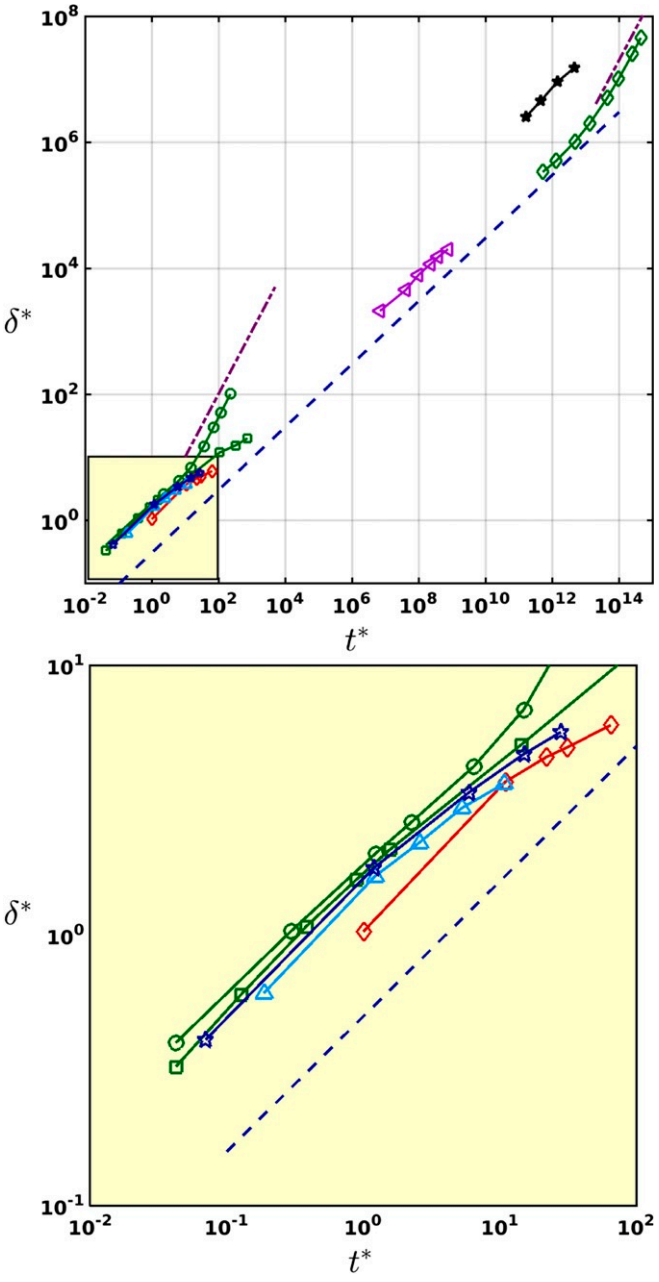

Fig. 2. Minimum distance between reconnecting vortices: past and present results. (*Top*) All data reported describe the behavior of the rescaled minimum distance δ^* between vortices as a function of the rescaled temporal distance to the reconnection event t^*. Open (solid) symbols refer to pre(post)reconnection dynamics. GP simulations: red ◊, ref. 50; blue ☆, ref. 48; turquoise △, ref. 38; green ○ and □, present simulations, ring–vortex collision and orthogonal reconnection, respectively. VF method simulations: purple ◁, ref. 44; green ◊, present simulations, ring–line collision. Experiments: ★, ref. 52. (*Bottom*) Zoom-in on GP simulations.

Numerical Simulations

There are two established models of quantum vortex dynamics: the Gross–Pitaevskii (GP) model and the vortex filament (VF) method. The former describes a weakly interacting BEC in the zero-temperature limit (58), and the latter is based on the classical Biot–Savart law describing the velocity field of a given vorticity distribution, which in our case is concentrated on space curves (59, 60).

The main difference between GP and VF models is the probed length scales of the flow. The GP equation is a microscopic, compressible model, capable of describing density fluctuations and length scales smaller than the vortex core a_0 (defined as the diameter of the cylindrical tube around the superfluid vortex line where the density is within 75% of the bulk density). In the GP model, vortices are identified as topological phase defects of the condensate wavefunction Ψ, and reconnections are solutions of the GP equation itself. On the other hand, the VF method is a mesoscopic incompressible model, probing the features of the flow at length scales much larger than the vortex core, typically $10^4\ a_0$ or $10^5\ a_0$, neglecting any density perturbation created by moving vortices and the density depletions represented by the vortex cores themselves. In the VF model, vortex lines are discretized using a set of Lagrangian points whose dynamics are governed by the classical Biot–Savart law, and vortex reconnections are performed by an ad hoc "cut-and-paste" algorithm (59, 61).

In the present study, we use both GP and VF models to investigate the scaling with time of the minimum distance δ between reconnecting vortices. Technical details of these methods are described in *SI Appendix*, sections SI.6 and SI.7. Distinctive of our simulations is the larger initial distance δ_0 compared with that in past numerical studies (5–20 times larger in GP simulations, and 100–2,000 times larger in VF ones). We also extend the use of the GP model to inhomogeneous, confined BECs where vortex reconnections can now be investigate experimentally with unprecedented resolution (21).

Homogeneous Unbounded Systems. To make progress in the understanding of vortex reconnections in homogenous quantum fluids, we identify two limiting initial vortex configurations which generate the two fundamental types of reconnections. The first configuration consists of two initially straight and orthogonal vortices, corresponding to the limit where the curvatures K_1 and K_2 of the two vortices are small and comparable (i.e., $K_1 \sim K_2$ and $K_1, K_2 \ll 1$); the second configuration is a vortex ring interacting with an isolated vortex line, which is the limiting case of two vortices of significantly different curvatures ($K_1 \ll K_2$ or $K_1 \gg K_2$). The third limiting case of large and comparable curvatures ($K_1 \sim K_2$ and $K_1, K_2 \gg 1$), i.e., the collision of small vortex rings, is neglected in the present study as it refers to an extremely unlikely event, due to the small cross-section.

The orthogonal reconnection configuration and the corresponding results for $\delta(t)$ are shown in Fig. 3 (*Left*) and reported in Movies S1–S4. Previous GP simulations of this geometry used initial distances $\delta_0 \lesssim 6\,\xi$, where $\xi = \hbar/\sqrt{2\ mgn}$ is the healing length of the system ($a_0 \approx 4\,\xi$ to $5\,\xi$), and m, g, and n are the boson mass, the repulsive strength of boson interaction, and the bulk density of bosons, respectively. Here we extend the investigations to initial distances $\delta_0 \approx 30\,\xi$. Introducing the rescaled distance $\delta^* = \delta/\xi$ and time $t^* = |t - t_r|/\tau$ (where t_r is the reconnection instant and $\tau = \xi/c$, with $c = \sqrt{gn/m}$ being the speed of sound in a homogeneous BEC), we observe that for $\delta^* \lesssim 2.5$ (when the two vortex lines are so close to each other that the condensate's density in the region between them is significantly less than the bulk density) a symmetrical $t^{*1/2}$ scaling emerges clearly for both pre- and postreconnection dynamics. This is consistent with the most recent GP simulations (48) and inconsistent with other numerical GP studies (38, 50), adding further evidence

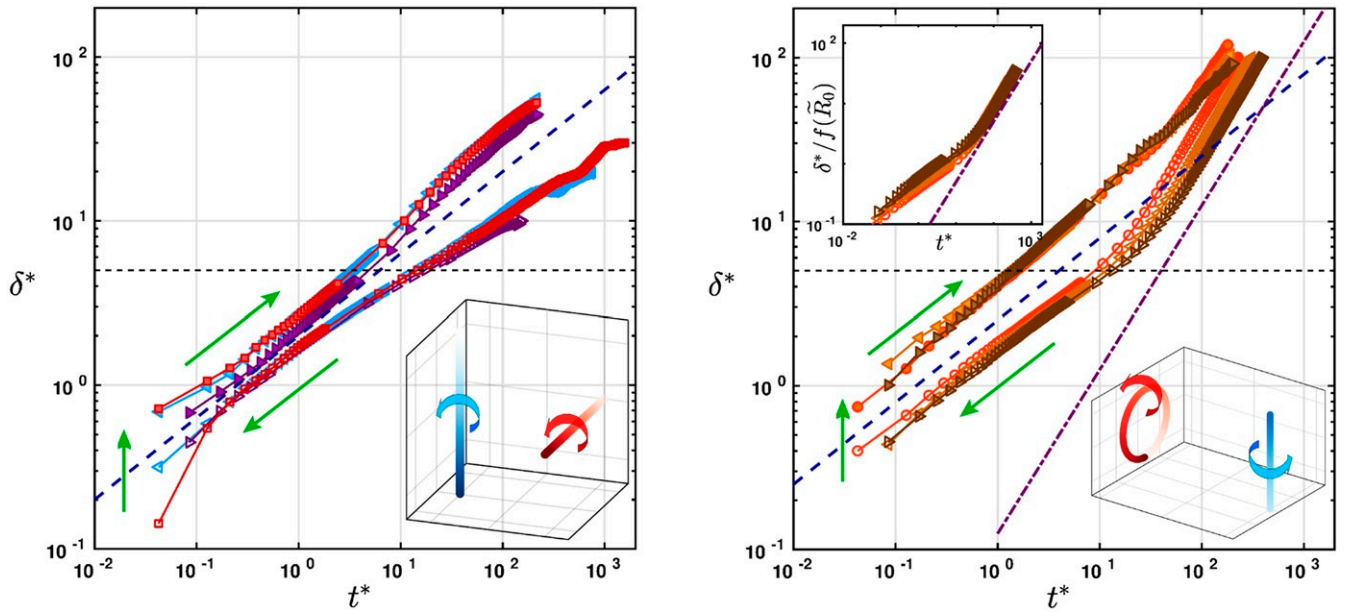

Fig. 3. GP simulations: homogeneous unbounded BECs. Shown is evolution of the rescaled minimum distance δ^* between reconnecting vortices as a function of the rescaled temporal distance to reconnection t^*. Open (solid) symbols correspond to pre(post)reconnection dynamics. (*Left*) Orthogonal vortices reconnection with rescaled initial distance δ_0^* equal to 10 (violet ▷), 20 (blue ◁), and 30 (red □). (*Right*) Ring–line reconnection for constant initial distance $\delta_0^* = 100$ and vortex ring radii R_0^* equal to 5 (orange ○), 7.5 (yellow ◁), and 10 (brown ▷). (*Top Inset*) Prereconnection dynamics only, where the distance is rescaled with $f(\tilde{R}_0)$. In both *Left* and *Right*, the horizontal dashed black line indicates the width of the vortex core ($\approx 5\,\xi$), the blue-dashed line shows the $t^{*1/2}$ scaling, and the *Bottom Insets* show the initial vortex configuration. Color gradient on vortices indicates direction of the superfluid vorticity (from light to dark). Dotted-dashed violet line (*Right*) indicates the t^* scaling. Green arrows indicate the direction of time.

to a $t^{*1/2}$ symmetrical scaling at small distances for orthogonal reconnections.

To map quantitatively the emergence of the $t^{*1/2}$ behavior in distinct intervals of δ, in Table 1 we report the scaling exponents α of the power-law fits $\delta^* \sim t^{*\alpha}$ for the intermediate initial distance $\delta_0^* = 20$. From Table 1 it clearly emerges that the $t^{*1/2}$ scaling also holds in the postreconnection dynamics at large distances, while in the intermediate region $2.5 < \delta^* < 10$ (both pre- and postreconnection) and at large distances during the approach, the scalings deviate from $t^{*1/2}$. To investigate these deviations, we calculate the velocity contribution of the local vortex curvature, v_γ, to the approach/separation velocity $d\delta^*/dt^*$ for the intermediate initial distance $\delta_0^* = 20$, displaying the corresponding results in Fig. 4, *Top* (see *SI Appendix*, section SI.2 for the calculation of v_γ). Fig. 4, *Top* clearly shows that the observed deviations from the $t^{*1/2}$ scaling depend on the relative curvature contribution $\sigma = v_\gamma/(d\delta^*/dt^*)$: The larger σ is, the more prominent the deviations are from the $t^{*1/2}$ behavior. This implies that the $t^{*1/2}$ scaling observed at large distances in the separation dynamics originates from an interaction-dominated motion of the reconnecting strands. If the dynamics are governed by the mutual interaction of the two vortices, in fact, $d\delta^*/dt^* \propto \kappa/(4\pi\delta^*)$ (44), leading straightforwardly to the scaling $\delta^* \sim t^{*1/2}$, derived in Eq. **2**. This argument corroborates the experimentally observed $t^{*1/2}$ scaling (46, 52). Concluding our study of orthogonal reconnections, we note that vortex lines move faster after the reconnection than before it, as pointed out in past studies (38, 48–50), and that the postreconnection curves show a slight sensitivity to the initial distance δ_0^*.

The second homogeneous system which we consider is a vortex ring reconnecting with an isolated initially straight vortex line (Movies S5–S8). This scenario is notably relevant in superfluid helium turbulence at low temperatures, where the low density of thermal excitations is not able to quickly damp out small vortex structures. In fact, the methods used to generate turbulence at low temperatures involve either injecting vortex rings (62–65) or vibrating small structures (e.g., spheres, wires, and grids) which trigger a great number of ring–line collisions (66–68). Similarly, also inhomogeneous quantum turbulence (69, 70) and boundary layer turbulence (71) display conspicuous vortex loop–vortex line collisions.

Fig. 3 (*Right*) illustrates this vortex setup and presents the behavior of $\delta(t)$. We vary the initial radius of the ring ($R_0^* = R_0/\xi = 5, 7.5$, and 10), while keeping constant its initial distance $\delta_0^* = 100$ to the line. We first focus on the prereconnection evolution of $\delta(t)$. This clearly reveals the two distinct scalings predicted by the dimensional analysis,

$$\delta^*(t^*) \sim a_{1/2}\, t^{*1/2} \quad \text{for} \quad t^* \lesssim 5, \qquad [5]$$

$$\delta^*(t^*) \sim a_1\, t^* \quad \text{for} \quad t^* \gtrsim 20, \qquad [6]$$

where $a_{1/2}$ and a_1 are constant prefactors corresponding, respectively, to $(C_1\kappa)^{1/2}$ in Eq. **2** and v_ℓ and v_{∇_ρ} in Eqs. **3** and **4**. To our knowledge, the linear scaling has not been reported in previous studies. We also note that the crossover between these two regimes occurs at a distance of $\delta_c \sim 3-4\,\xi$; we will revisit the importance of this scale later.

Table 1. GP simulations: homogeneous unbounded BECs, orthogonal reconnection

	$\delta^* < 2.5$	$2.5 < \delta^* < 10$	$\delta^* > 10$
α^-	0.48	0.40	0.43
α^+	0.49	0.60	0.50

Shown are scaling exponents α^- (α^+) for power-law behavior $\delta^* \sim t^{*\alpha}$ for pre(post)reconnection dynamics for initial separation $\delta_0^* = 20$.

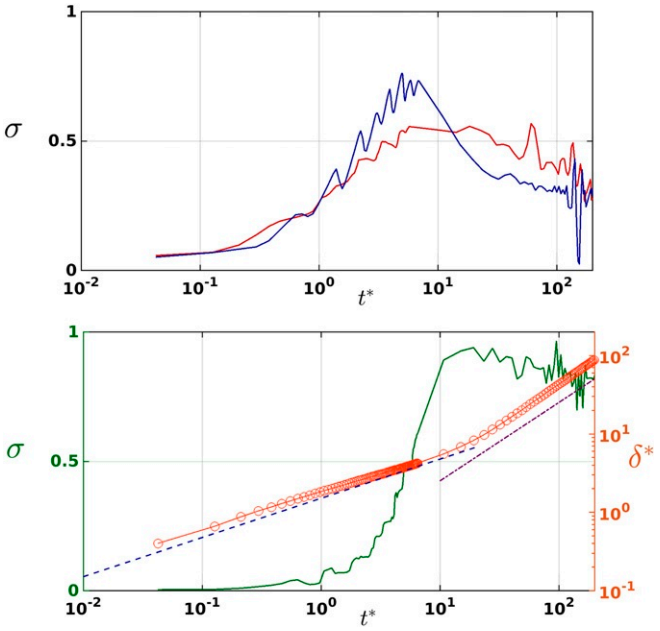

Fig. 4. Curvature contribution. (*Top*) Temporal evolution of the ratio σ for the orthogonal reconnection with initial separation distance $\delta_0^* = 20$. Red (blue) symbols correspond to pre(post)reconnection dynamics. (*Bottom*) Temporal evolution of σ (green solid line) and rescaled minimum distance δ^* (orange circles) for the ring–line prereconnection, with $R_0^* = 5$. The dashed blue line shows the $t^{*1/2}$ scaling, while the dotted-dashed violet line indicates the t^* scaling.

The linear scaling implies that $d\delta^*/dt^*$ is constant: At large distances, the relative velocity between the two points at minimum distance, $\mathbf{x}_{\rm ring}$ (on the vortex ring) and $\mathbf{x}_{\rm line}$ (on the vortex line), projected on the separation vector $\boldsymbol{\delta} = \mathbf{x}_{\rm ring} - \mathbf{x}_{\rm line}$, is constant with respect to time. We argue that, at large separation distances, $d\delta^*/dt^*$ is approximately equal to the initial speed of the vortex ring (72):

$$\frac{d\delta^*}{dt^*} = v_{\rm ring}^* = \frac{\kappa}{4\pi\xi c R_0^*}\left[\ln(8R_0^*) - 0.615\right]. \qquad [7]$$

The self-induced velocity of the vortex ring $v_{\rm ring}$ thus plays the role of the characteristic velocity v_ℓ in Eq. **3**. We make the notation compact and rewrite Eq. **7** as $v_{\rm ring}^* = Cf(\widetilde{R}_0)$, where $C = \kappa/(4\pi c\overline{R}_0)$, $f(\widetilde{R}_0) = [\ln(\widetilde{R}_0) + 3.48]/\widetilde{R}_0$, $\overline{R}_0 = 7.5\,\xi$ is the average radius of the three simulations, and $\widetilde{R}_0 = R_0/\overline{R}_0$. We then arrive at the result that Eq. **6** takes the form $\delta^*(t^*) \sim Cf(\widetilde{R}_0)\, t^*$. This is confirmed in Fig. 3, *Right*, *Top Inset*: When δ^* is rescaled as $\delta^*/f(\widetilde{R}_0)$, the curves collapse onto a single curve in the $\delta \sim t$ regime. The clear $t^{*1/2}$ scaling for $\delta^* \lesssim \delta_c^*$ is consistent with the interpretation put forward for the orthogonal reconnection, as at such small distances, the approach/separation is likely to be governed by the mutual interaction of the two vortices given that δ is smaller than the ring's radius of curvature.

We hence suggest that these two scalings correspond to a crossover from dynamics predominantly driven by mutual vortex interaction ($\delta^* \sim t^{*1/2}$ scaling) to the self-driven (curvature-driven) motion of the ring ($\delta^* \sim t^*$ scaling). To check this

conjecture, we again refer to the contribution of the local vortex curvature: Fig. 4, *Bottom* shows the relative curvature contribution for the ring–line prereconnection dynamics. We see that the contribution from the local vortex curvature to the approach velocity drops dramatically for $t^* \lesssim 5$, corresponding exactly to the onset of the $t^{*1/2}$ scaling, supporting this picture.

The crossover between the two scalings, however, is less apparent in the postreconnection dynamics and for two main reasons. First, both vortices become perturbed by propagating Kelvin waves; second, the traveling velocity of the perturbed vortex ring is not constant (73–75). These Kelvin waves generate sound waves (76, 77) dissipating the incompressible kinetic energy, leading to a decrease of the length of the vortex ring and a damping of the oscillations' amplitude. When these oscillations die out (e.g., in the simulation with $R_0^* = 5$; Fig. 3, *Right*), and the vortex ring regains its circular shape traveling at constant velocity away from the vortex line, we recover the expected $\delta^* \sim t^*$ scaling. These wobbling dynamics and the recovery of the linear scaling are addressed in more detail in *SI Appendix*, section SI.3.

The same qualitative behavior for the orthogonal vortices and ring–line scenario is recovered in VF simulations (*SI Appendix*, section SI.4 and Fig. S2). In the latter scenario, the crossover from $t^{*1/2}$ to t^* scaling occurs at much larger length scales than in the GP simulations, given the range of scales involved ($\approx 10^5 a_0 - 10^8 a_0$). However, as for GP simulations, the distance δ_c at which the crossover takes place is determined by the balance between interaction-dominated motion and curvature-driven dynamics, i.e., by the comparison between $\delta(t)$ and the radius of curvature $R_c(t)$ of the vortex ring.

Trapped Systems. Since it is now experimentally possible to visualize individual quantum reconnections in trapped atomic BECs (21, 78), we test the above results under such realistic experimental setups. We consider two classes of traps: the widely used harmonic traps (79) (Figs. 5 and 6 and Movies S9 and S10) and the recently designed box traps (80, 81) (*SI Appendix*, section SI.5 and Movies S11 and S12). We use GP simulations throughout this analysis (the VF model is not suitable for inhomogeneous systems).

In harmonic traps the condensate is inhomogeneous (the density is larger near the center) and individual motion of the vortices (responsible for the linear scaling) is determined by their curvature, density gradients, and possibly vortex images (56, 57, 82, 83). In box traps the condensate's density is constant (with the exception of a thin layer of width of the order of the healing length near the boundary), and the individual vortex motion is believed to be driven by image vortices with respect to the boundaries, according to 2D studies (84). We exploit these self-driven vortex motions to analyze reconnections starting from initial distances significantly larger than those in previous numerical simulations (up to 20 times larger).

Consider first the harmonic trap case; the initial configuration is shown in Fig. 5. The condensate is taken to be cigar shaped, with the long axis along x (the trapping frequency ω_x along x is smaller than those in the transverse directions, $\omega_y = \omega_z = \omega_\perp$). In this geometry, a single straight vortex line imprinted off center on a radial plane is known to orbit around the center of the condensate (85, 86) along an elliptical orbit perpendicular to itself. The vortex follows a trajectory of constant energy (57) which is uniquely determined by the orbit parameter $\chi = x_0/R_x = r_0/R_\perp$, where x_0 and r_0 are the axial and radial semiaxes of the ellipse, and R_x and $R_\perp$ are the axial and radial Thomas–Fermi radii, respectively. The period T of this orbit decreases with increasing χ (57, 78, 83, 87, 88), $T = \frac{8\pi\left(1-\chi^2\right)\mu}{3\hbar\omega_\perp\omega_x \ln(R_\perp/\xi_c)}$, where ξ_c is the healing length at the center of the trap. Hence, outer vortices (with larger values of χ) move faster.

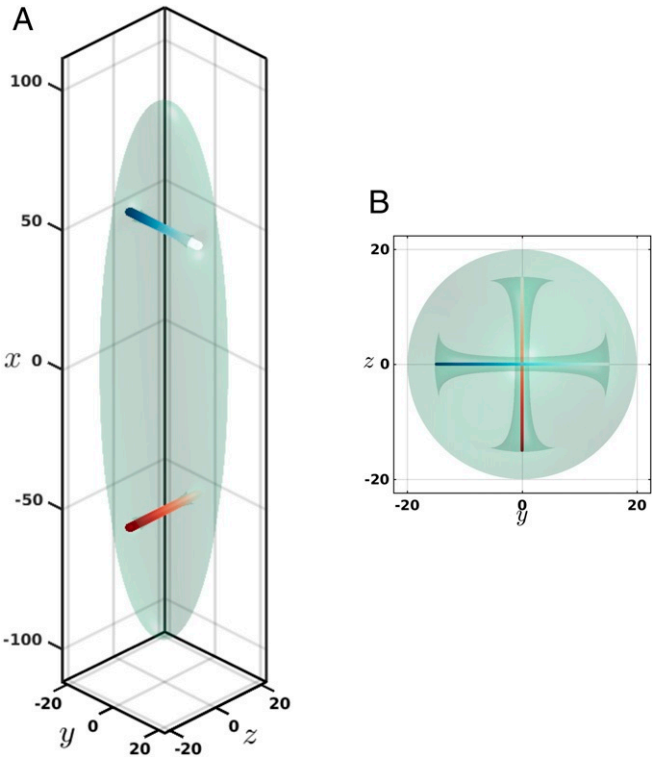

Fig. 5. GP simulations: harmonically trapped BECs, initial conditions. (*A* and *B*) Lateral (*A*) and top (*B*) views of initial vortex configuration. Light green surfaces are isosurfaces of condensate density at 5% of trap-center density. Color gradient on vortices indicates the direction of the superfluid vorticity (from light to dark). Unit of length is the healing length ξ_c evaluated in the center of the trap.

If two orthogonal vortices are imprinted on radial planes, intersecting the (long) x axis at opposite positions $\pm x_0$, distinct vortex interactions can occur (vortex rebounds, vortex reconnections, double reconnections, ejections), depending on the value of the orbit parameter χ (21). Results presented here refer to three different values of χ, all engendering vortex reconnections: $\chi = 0.35,\ 0.5,\ 0.6$. The prereconnection evolution of $\delta^* = \delta/\xi_c$ is reported in Fig. 6, *Left*. As for the ring–line reconnection, we observe a crossover from $t^{*1/2}$ to t^* scaling. This occurs for all values of χ. Moreover, the $t^{*1/2}$ scaling again occurs in the region $\delta^* \lesssim 5$, suggesting that this feature is indeed universal for vortex reconnections in BECs.

If we rescale the minimum distance δ with the healing length ξ_r evaluated at the reconnection point $\mathbf{x}_r$, $\xi_r = \frac{\hbar}{\sqrt{2gmn_{\mathrm{TF}}(\mathbf{x}_r)}}$ ($n_{\mathrm{TF}}(\mathbf{x}_r)$ being the condensate particle density according to the Thomas–Fermi approximation), the curves corresponding to distinct values of χ overlap for $\delta_r^* = \delta/\xi_r \lesssim 5$ (Fig. 6, *Right Inset*). This result implies that ξ_r (hence the radius of the vortex core) is the correct length scale which characterizes the approach dynamics when vortex cores start merging. Furthermore, the dependence of ξ_r on $mn_{\mathrm{TF}}(\mathbf{x}_r)$ indicates that mass density $\rho = mn$ itself plays a significant role in determining the minimum distance δ—this is exactly why we included ρ in the set of physical variables when applying Buckingham's π-theorem.

Another similarity between reconnections in harmonic traps and other geometries is the faster postreconnection dynamics, as seen in Fig. 6, *Left Inset*. This velocity difference between approach and separation (related to an increase of the local vor-

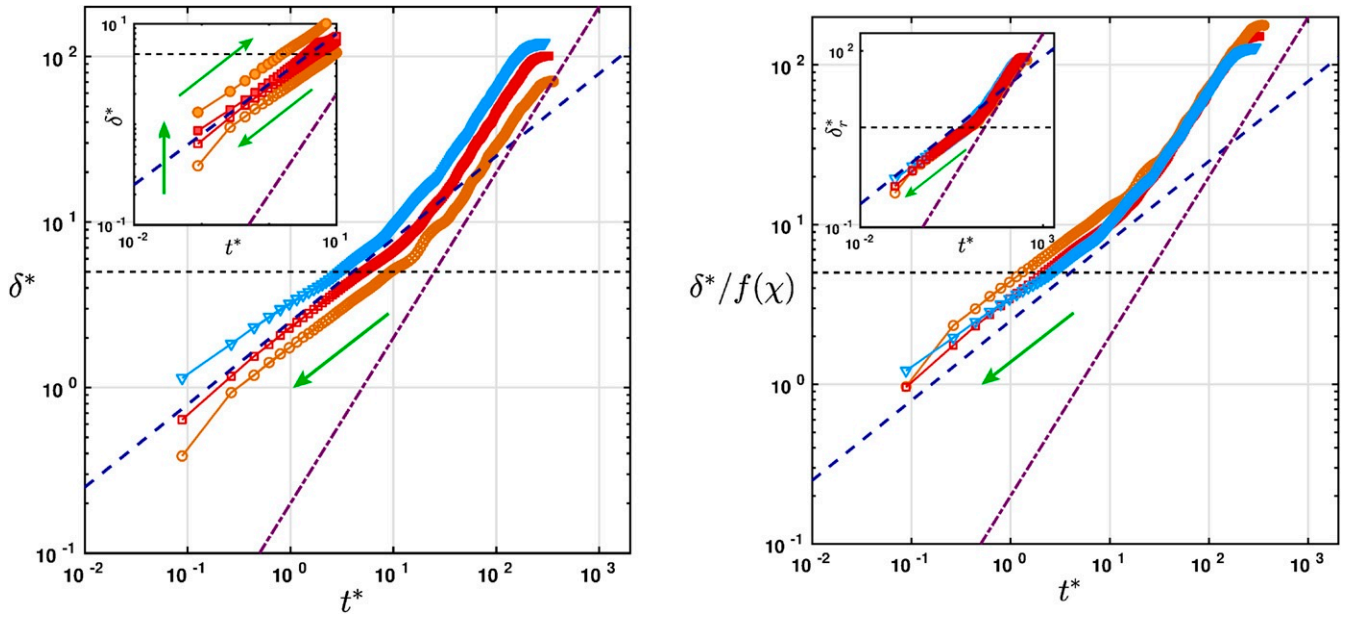

Fig. 6. GP simulations: harmonically trapped BECs. Shown is evolution of the minimum distance δ^* between reconnecting vortices as a function of the temporal distance to reconnection t^*. Open (solid) symbols correspond to pre(post)reconnection dynamics. (*Left*) Prereconnection scaling of δ^* for initially imprinted orthogonal vortices with corresponding orbit parameter $\chi = 0.35$ (yellow ○), $\chi = 0.5$ (red □), and $\chi = 0.6$ (blue ▽). *Inset* shows short-time prereconnection (open symbols) and postreconnection (solid symbols) scaling of δ^* for $\chi = 0.35$ (yellow ○) and $\chi = 0.5$ (red □). (*Right*) Temporal evolution of the minimum distance δ^* rescaled with $f(\chi)$. Symbols are as in *Left* panel. *Inset* shows short-time prereconnection scaling of rescaled minimum distance $\delta^*_r = \delta/\xi_r$. In both *Left* and *Right*, the dashed blue and dotted-dashed violet lines show the $t^{*1/2}$ and t^* scalings, respectively. The horizontal dashed line indicates the width of the vortex core at the center of the trap ($\approx 5\,\xi$). Green arrows indicate the direction of time.

tex curvature in the reconnection process and to an emission of acoustic energy) seems a universal feature of quantum vortex reconnections (48) and is also observed in simulations of reconnecting classical vortex tubes (51).

Fig. 6, *Left* shows that $\frac{d\delta^*}{dt^*}$ is constant for $t^* \gtrsim 20$ before the reconnection, increasing with increasing values of the orbital parameter χ (this is not surprising since isolated vortices move faster on outer orbits). It seems reasonable to assume that $\frac{d\delta^*}{dt^*} = Cf(\chi)$, where $f(\chi) = \frac{\chi}{1-\chi^2}$ and C is a constant which depends on the trap's geometry. Indeed, the magnitude of the vortex velocity induced by both density gradients (57, 82, 89) and vortex curvature (assuming, for simplicity, that the shape of the vortex is an arc of a circle) is proportional to $f(\chi)$. As a consequence, we expect that $\delta^*(t^*) \sim Cf(\chi)\, t^*$ for $t^* \gtrsim 20$. This conjecture is confirmed in Fig. 6, *Right*: When plotted as $\delta^*/f(\chi)$, the curves for different χ collapse onto a universal curve in this region.

We stress that the observed linear scaling at large distances is a result that, to our knowledge, has not been observed previously in literature. However, although we have numerically identified the dependence of $d\delta^*/dt^*$ on χ at large distances, we still lack a simple physical justification of this result.

In harmonic traps, the predominant effect driving the approach of the vortices at large distances is hence the individual vortex motion driven by curvature and density gradients (the role of vortex images still remains unclear (83) in this trap geometry), independent of the presence of the other vortex. The scaling crossover in harmonic traps is thus governed by the balance between the interaction of the reconnecting strands and the driving of the individual vortices, as it occurs for the ring–line reconnection in homogeneous BECs described previously.

The nature of this scaling crossover is confirmed by the investigation of vortex reconnections in box-trapped BECs, outlined in *SI Appendix*, section SI.5 and Fig. S4. In these trapped systems, the motion of individual vortices is found to be driven by vortex images, leading to a linear scaling at large distances. At small distance we again recover the $\delta \sim t^{*1/2}$ scaling. The results obtained in all of the trapped BECs investigated in this work,

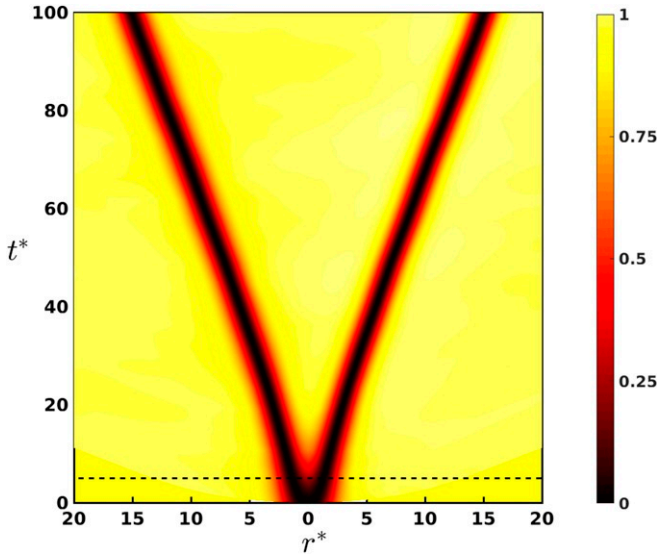

Fig. 7. The role of density depletions. Shown is a plot of the condensate density along the line containing the separation vector $\boldsymbol{\delta}$ between the colliding vortices, as a function of the distance r^* to the midpoint of the separation segment and the rescaled temporal distance to reconnection t^*, for the vortex ring–vortex line prereconnection dynamics with $R_0^* = 5$. In the initial phase of the approach (top part), $\delta \sim t^*$; the crossover to the $\delta \sim t^{*1/2}$ scaling occurs when the vortex cores start to merge (bottom part) for $t^* \lesssim 5$ (dashed line).

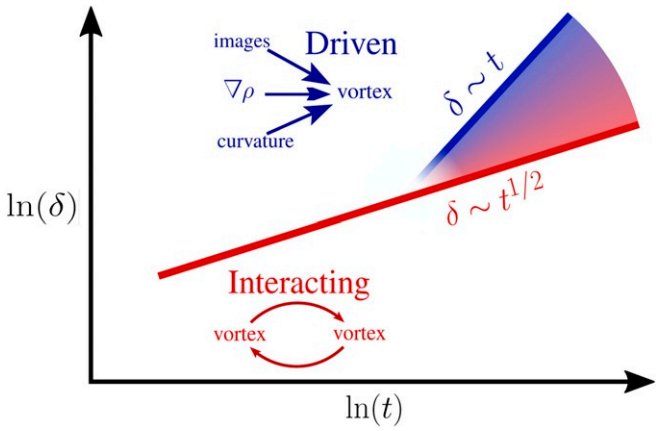

Fig. 8. Fundamental scalings for the reconnection of two vortex lines. At small length scales the $\delta^* \sim t^{*1/2}$ scaling (in red) is observed as the dynamics are determined by the mutual interaction of the two reconnecting vortex strands. This scaling appears to be universal. At larger distances, we observe two fundamental limiting scenarios: If the motion is still predominantly driven by the interaction, the $\delta^* \sim t^{*1/2}$ scaling (in red) still holds; if the dynamics are governed by extrinsic factors driving the individual vortices, a linear $\delta^* \sim t^*$ behavior is established (in blue). In this last case, a scaling crossover occurs. At large distances, intermediate scalings can arise due to additional physics, e.g., Kelvin waves (in red–blue color gradient).

hence, always show a $\delta \sim t^{*^{1/2}}$ to $\delta \sim t^*$ scaling crossover which, we stress, has not been observed in past studies. In addition, the always observed small-scale $\delta \sim t^{*^{1/2}}$ behavior supports the argument for the existence of a universal scaling law at length scales close to the reconnection point.

The Role of Density Depletions. Current and previous GP simulations of reconnections in homogeneous and trapped BECs show a clear symmetric pre/postreconnection $t^{*^{1/2}}$ scaling in the region $\delta^* \lesssim 5$, irrespective of the initial condition. The effect is robust and mostly went unnoticed, as the prefactors $a_{1/2}$ in Eq. **5** may vary, depending on the conditions and between the approach/separation.

Fig. 7 shows the condensate density along the line containing the separation vector between two reconnecting vortices (taken to be the ring–line scenario in a homogeneous system), as a function of t^* and the distance $r^* = r/\xi$ to the midpoint of the separation segment. It is clear that for $t^* \lesssim 5$, which is when the $t^{*^{1/2}}$ scaling appears, the density between the two vortices drops dramatically. This behavior is generic—we obtain it also for any vortex reconnection setup and across homogeneous and trapped BECs. This result confirms the analytical work of Nazarenko and West (18), who Taylor expanded the solution of the GP for reconnecting vortex lines and predicted the observed $t^{1/2}$ scaling in this limit of vanishing density (in this limit the cubic nonlinear term vanishes, reducing the GP equation to the linear Schrödinger equation). There are hence two different arguments for the observation of the $t^{1/2}$ scaling: the interaction-driven dynamics argument, underlying the dimensional scaling of Eq. **2**, and the vanishing density argument from the GP equation. The arguments are both valid at small length scales, consistent with the $t^{1/2}$ scaling observed close to reconnection in all GP simulations.

Conclusions

We have addressed the question of whether there is a universal route to quantum vortex reconnections by performing an extensive campaign of numerical simulations using the two main mathematical models available (the Gross–Pitaevskii equation and vortex filament method). What distinguishes our work from previous studies is that, first, we have studied the two main physical systems which display quantized vorticity (trapped atomic condensates and superfluid helium) and, second, we have considered the behavior over distances one order of magnitude larger. By applying rigorous dimensional arguments, we have found that the minimum distance between reconnecting vortex lines may obey two fundamental scaling-law regimes: the already observed $\delta^* \sim t^{*^{1/2}}$ scaling and also a $\delta^* \sim t^*$ scaling.

At small length scales, we always observe the $\delta^* \sim t^{*^{1/2}}$ scaling; this arises from either the mutual interaction between reconnecting strands or the depleted density/nonlinearity in the reconnection region. The observation of this scaling in all GP simulations, independent of the precise nature of the system (homogeneous or trapped) and initial vortex configuration, adds further evidence for the existence of this universal $\delta^* \sim t^{*^{1/2}}$ scaling law close to reconnection. At larger length scales, two fundamental limiting cases appear: the continuation of the $\delta^* \sim t^{*^{1/2}}$ scaling if the dynamics are still governed by the vortex mutual interaction or a linear $\delta^* \sim t^*$ behavior if vortices are individually driven by extrinsic factors, such as curvature, density gradients, and boundaries/images. In the latter case, the crossover between the two scaling regimes is determined by the balance between interaction-dominated motion and individually driven dynamics. This scaling behavior is summarized schematically in Fig. 8. We stress that these two fundamental scaling laws represent limiting behaviors: Intermediate scalings can arise due to additional physics, e.g., Kelvin waves. We also stress that the $\delta^* \sim t^*$ cannot arise from a uniform flow, which would simply advect both vortices in the same direction. Instead, it arises in distinct systems, both homogeneous and inhomogeneous, from the different illustrated physical mechanisms and has not yet been reported in the literature.

While in homogeneous systems the $t^{*^{1/2}}$ behavior can persist to arbitrary separations (e.g., for initially orthogonal and weakly curved vortices), we find that in trapped condensates the scaling crossover always arises. Indeed, the current technological ability to directly image vortex lines in trapped condensates suggests that full 3D reconstructions will soon be available, putting the detection of this crossover within experimental reach.

Materials and Methods

The two numerical methods which we use, the GP equation and the VF method, are standard and have already been described in the literature. The main features and some technical details peculiar to this problem are described in *SI Appendix*.

ACKNOWLEDGMENTS. L.G., C.F.B., and N.G.P. acknowledge the support of the Engineering and Physical Sciences Research Council (Grant EP/R005192/1).

1. E. Priest, T. Forbes, *Magnetic Reconnection: MHD Theory and Applications* (Cambridge University Press, 2007).
2. H. Che, J. Drake, M. Swisdak, A current filamentation mechanism for breaking magnetic field lines during reconnection. *Nature* **474**, 184–187 (2011).
3. J. W. Cirtain *et al.*, Energy release in the solar corona from spatially resolved magnetic braids. *Nature* **493**, 501–503 (2013).
4. I. Chuang, R. Durrer, N. Turok, B. Yurke, Cosmology in the laboratory: Defect dynamics in liquid crystals. *Science* **251**, 1336–1342 (1991).
5. D. Sumners, Lifting the curtain: Using topology to probe the hidden action of enzymes. *Notice AMS* **42**, 528 (1995).
6. M. Vazques, D. Sumners, Tangles analysis of gin site-specific recombination. *Math. Proc. Camb. Philos. Soc.* **136**, 565–582 (2004).
7. M. Dennis, R. King, B. Jack, K. O'Holleran, M. Padgett, Isolated optical vortex knots. *Nat. Phys.* **6**, 118–121 (2010).
8. M. Berry, M. Dennis, Reconnections of wave vortex lines. *Eur. J. Phys.* **33**, 723–731 (2012).

9. S. Kida, M. Takaoka, Vortex reconnection. *Annu. Rev. Fluid Mech.* **26**, 169–177 (1994).
10. A. Pumir, R. Kerr, Numerical simulation of interacting vortex tubes. *Phys. Rev. Lett.* **58**, 1636–1639 (1987).
11. D. Kleckner, W. T. Irvine, Creation and dynamics of knotted vortices. *Nat. Phys.* **9**, 253–258 (2013).
12. C. Barenghi, R. Donnelly, W. Vinen, *Quantized Vortex Dynamics and Superfluid Turbulence* (Springer, 2001).
13. K. Schwarz, Three-dimensional vortex dynamics in superfluid he4: Homogeneous superfluid turbulence. *Phys. Rev. B* **38**, 2398–2417 (1988).
14. L. Onsager, Statistical hydrodynamics. *Nuovo Cim.* **6** (suppl. 2), 279–287 (1949).
15. R. Feynmann, *Application of Quantum Mechanics to Liquid Helium* (North Holland Publ. Co., 1955), Vol. **1**, p. 36.
16. W. Vinen, The detection of single quanta of circulation in liquid helium II. *Proc. R. Soc. Lond. Ser. A* **260**, 218–236 (1961).
17. R. J. Donnelly, *Quantized Vortices in Helium II* (Cambridge University Press, 1991).
18. S. Nazarenko, R. West, Analytical solution for nonlinear Schrödinger vortex reconnection. *J. Low Temp. Phys.* **132**, 1 (2003).
19. J. Koplik, H. Levine, Vortex reconnection in superfluid helium. *Phys. Rev. Lett.* **71**, 1375–1378 (1993).
20. G. Bewley, M. Paoletti, K. Sreenivasan, D. Lathrop, Characterization of reconnecting vortices in superfluid helium. *Proc. Natl. Acad. Sci. U.S.A.* **105**, 13707–13710 (2008).
21. S. Serafini *et al.*, Vortex reconnections and rebounds in trapped atomic Bose-Einstein condensates. *Phys. Rev. X* **7**, 021031 (2017).
22. C. Barenghi, V. L'vov, P. Roche, Experimental, numerical and analytical velocity spectra in turbulent quantum fluid. *Proc. Natl. Acad. Sci. U.S.A.* **111** (suppl. 1), 4683–4690 (2014).
23. A. Baggaley, J. Laurie, C. Barenghi, Vortex-density fluctuations, energy spectra, and vortical regions in superfluid turbulence. *Phys. Rev. Lett.* **109**, 205304 (2012).
24. C. Nore, M. Abid, M. Brachet, Kolmogorov turbulence in low-temperature superflows. *Phys. Rev. Lett.* **78**, 3896–3899 (1997).
25. L. Skrbek, K. Sreenivasan, Developed quantum turbulence and its decay. *Phys. Fluids* **24**, 011301 (2012).
26. J. Maurer, P. Tabeling, Local investigation of superfluid turbulence. *Europhys. Lett.* **43**, 29–34 (1998).
27. J. Salort *et al.*, Turbulent velocity spectra in superfluid flows. *Phys. Fluids* **22**, 125102 (2010).
28. D. Kleckner, L. Kauffman, W. Irvine, How superfluid vortex knots untie. *Nat. Phys.* **12**, 650–655 (2016).
29. M. Scheeler, D. Kleckner, D. Proment, G. Kindlmann, W. Irvine, Helicity conservation by flow across scales in reconnecting vortex links and knots. *Proc. Natl. Acad. Sci. U.S.A.* **111**, 15350–15355 (2014).
30. P. Di Leoni, P. D. Mininni, M. E. Brachet, Helicity, topology and Kelvin waves in reconnecting quantum knots. *Phys. Rev. A* **94**, 043605 (2016).
31. H. Salman, Helicity conservation and twisted Seifert surfaces for superfluid vortices. *Proc. R. Soc. A* **473**, 20160853 (2017).
32. C. F. Barenghi, L. Galantucci, N. G. Parker, A. W. Baggaley, Classical helicity of superfluid helium. arXiv:1805.09005 (23 May 2018).
33. C. Laing, R. Ricca, D. Sumners, Conservation of writhe helicity under anti-parallel reconnection. *Sci. Rep.* **5**, 9224 (2015).
34. S. Zuccher, R. Ricca, Helicity conservation under quantum reconnection of vortex rings. *Phys. Rev. E* **92**, 061001 (2015).
35. S. Zuccher, R. L. Ricca, Relaxation of twist helicity in the cascade process of linked quantum vortices. *Phys. Rev. E* **95**, 053109 (2017).
36. R. Hänninen, N. Hietala, H. Salman, Helicity within the vortex filament model. *Sci. Rep.* **6**, 37571 (2016).
37. M. Leadbeater, T. Winiecki, D. Samuels, C. Barenghi, C. Adams, Sound emission due to superfluid vortex reconnections. *Phys. Rev. Lett.* **86**, 1410–1413 (2001).
38. S. Zuccher, M. Caliari, A. Baggaley, C. Barenghi, Quantum vortex reconnections. *Phys. Fluids* **24**, 125108 (2012).
39. D. Kivotides, J. Vassilicos, D. Samuels, C. Barenghi, Kelvin waves cascade in superfluid turbulence. *Phys. Rev. Lett.* **86**, 3080–3083 (2001).
40. E. Kozik, B. Svistunov, Kelvin-wave cascade and decay of superfluid turbulence. *Phys. Rev. Lett.* **92**, 035301 (2004).
41. E. Kozik, B. Svistunov, Scale-separation scheme for simulating superfluid turbulence: Kelvin-wave cascade. *Phys. Rev. Lett.* **94**, 025301 (2005).
42. R. Kerr, Vortex stretching as a mechanism for quantum kinetic energy decay. *Phys. Rev. Lett.* **106**, 224501 (2011).
43. M. Kursa, K. Bajer, T. Lipniaki, Cascade of vortex loops initiated by a single reconnection of quantum vortices. *Phys. Rev. B* **83**, 014515 (2011).
44. A. De Waele, R. Aarts, Route to vortex reconnection. *Phys. Rev. Lett.* **72**, 482–485 (1994).
45. R. Tebbs, A. J. Youd, C. Barenghi, The approach to vortex reconnection. *J. Low Temp. Phys.* **162**, 314–321 (2011).
46. M. Paoletti, M. E. Fisher, D. Lathrop, Reconnection dynamics for quantized vortices. *Phys. D Nonlinear Phenom.* **239**, 1367–1377 (2010).
47. F. E. A. dos Santos, Hydrodynamics of vortices in Bose-Einstein condensates: A defect-gauge field approach. *Phys. Rev. A* **94**, 063633 (2016).
48. A. Villois, D. Proment, G. Krstulovic, Universal and nonuniversal aspects of vortex reconnections in superfluids. *Phys. Rev. Fluids* **2**, 044701 (2017).
49. A. Allen *et al.*, Vortex reconnections in atomic condensates at finite temperature. *Phys. Rev. A* **90**, 013601 (2014).
50. C. Rorai, J. Skipper, R. Kerr, K. Sreenivasan, Approach and separation of quantum vortices with balanced cores. *J. Fluid Mech.* **808**, 641–667 (2016).
51. F. Hussain, K. Duraisamy, Mechanics of viscous vortex reconnection. *Phys. Fluids* **23**, 021701 (2011).
52. E. Fonda, K. Sreenivasan, D. Lathrop, Reconnection scaling in quantum fluids. *Proc. Natl. Acad. Sci. U.S.A.* **116**, 1924–1928 (2019).
53. E. Fonda, D. Meichle, N. Ouellette, S. Hormoz, D. Lathrop, Direct observation of Kelvin waves excited by quantized vortex reconnection. *Proc. Natl. Acad. Sci. U.S.A.* **111** (suppl. 1), 4707–4710 (2014).
54. T. Lipniacki, Evolution of quantum vortices following reconnection. *Eur. J. Mech. B Fluids* **19**, 361–378 (2000).
55. E. Buckingham, On physically similar systems; illustrations of the use of dimensional equations. *Phys. Rev.* **4**, 345–376 (1914).
56. B. Jackson, J. McCann, C. Adams, Vortex line and ring dynamics in a trapped Bose-Einstein condensate. *Phys. Rev. A* **61**, 013604 (1999).
57. A. Svidzinsky, A. Fetter, Stability of a vortex in a trapped Bose-Einstein condensate. *Phys. Rev. Lett.* **84**, 5919–5923 (2000).
58. L. P. Pitaevskii, S. Stringari, *Bose-Einstein Condensation* (Oxford University Press, 2003).
59. K. Schwarz, Three-dimensional vortex dynamics in superfluid He 4: Line-line and line-boundary interactions. *Phys. Rev. B* **31**, 5782–5802 (1985).
60. Hänninen R, Baggaley A, Vortex filament method as a tool for computational visualization of quantum turbulence. *Proc. Natl. Acad. Sci. U.S.A.* **111** (suppl. 1), 4667–4674 (2014).
61. A. Baggaley, The sensitivity of the vortex filament method to different reconnection models. *J. Low Temp. Phys.* **168**, 18–30 (2012).
62. P. Walmsley, A. Golov, Quantum and quasiclassical types of superfluid turbulence. *Phys. Rev. Lett.* **100**, 245301 (2008).
63. P. Walmsley, P. Tompsett, D. Zmeev, A. Golov, Reconnections of quantized vortex rings in superfluid He 4 at very low temperatures. *Phys. Rev. Lett.* **113**, 125302 (2014).
64. D. Zmeev *et al.*, Dissipation of quasiclassical turbulence in superfluid He 4. *Phys. Rev. Lett.* **115**, 155303 (2015).
65. P. Walmsley, A. Golov, Coexistence of quantum and classical flows in quantum turbulence in the t = 0 limit. *Phys. Rev. Lett.* **118**, 134501 (2017).
66. R. Hänninen, M. Tsubota, W. Vinen, Generation of turbulence by oscillating structures in superfluid helium at very low temperatures. *Phys. Rev. B* **75**, 064502 (2007).
67. R. Goto *et al.*, Turbulence in boundary flow of superfluid He 4 triggered by free vortex rings. *Phys. Rev. Lett.* **100**, 045301 (2008).
68. A. Nakatsuji, M. Tsubota, H. Yano, Statistics of vortex loops emitted from quantum turbulence driven by an oscillating sphere. *Phys. Rev. B* **89**, 174520 (2014).
69. S. K. Nemirovskii, Diffusion of inhomogeneous vortex tangle and decay of superfluid turbulence. *Phys. Rev. B* **81**, 064512 (2010).
70. C. F. Barenghi, D. C. Samuels, Evaporation of a packet of quantized vorticity. *Phys. Rev. Lett.* **89**, 155302 (2002).
71. G. Stagg, N. Parker, C. Barenghi, Superfluid boundary layer. *Phys. Rev. Lett.* **118**, 135301 (2017).
72. P. H. Roberts, J. Grant, Motions in a Bose condensate. I. The structure of the large circular vortex. *J. Phys. A Gen. Phys.* **4**, 55–72 (1971).
73. R. Arms, F. R. Hama, Localized-induction concept on a curved vortex and motion of an elliptic vortex ring. *Phys. Fluids* **8**, 553–559 (1965).
74. M. Dhanak, B. D. Bernardinis, The evolution of an elliptic vortex ring. *J. Fluid Mech.* **109**, 189–216 (1981).
75. C. Barenghi, R. Hänninen, M. Tsubota, Anomalous translational velocity of vortex ring with finite-amplitude Kelvin waves. *Phys. Rev. E* **74**, 046303 (2006).
76. V. Kopiev, S. Chernyshev, Vortex ring eigen-oscillations as a source of sound. *J. Fluid Mech.* **341**, 19–57 (1997).
77. N. Parker, N. Proukakis, C. Barenghi, C. Adams, Controlled vortex-sound interactions in atomic Bose-Einstein condensates. *Phys. Rev. Lett.* **92**, 160403 (2004).
78. S. Serafini *et al.*, Dynamics and interaction of vortex lines in an elongated Bose-Einstein condensate. *Phys. Rev. Lett.* **115**, 170402 (2015).
79. F. Dalfovo, S. Giorgini, L. P. Pitaevskii, S. Stringari, Theory of Bose-Einstein condensation in trapped gases. *Rev. Mod. Phys.* **71**, 463–512 (1999).
80. A. Gaunt, T. Schmidutz, I. Gotlibovych, R. P. Smith, Z. Hadzibabic, Bose-Einstein condensation of atoms in a uniform potential. *Phys. Rev. Lett.* **110**, 200406 (2013).
81. N. Navon, A. Gaunt, R. P. Smith, Z. Hadzibabic, Emergence of a turbulent cascade in a quantum gas. *Nature* **539**, 72–75 (2016).
82. A. Fetter, A. Svidzinsky, Vortices in a trapped dilute Bose–Einstein condensate. *J. Phys. Condens. Matter* **13**, R135–R194 (2001).
83. A. Fetter, Rotating trapped Bose-Einstein condensates. *Rev. Mod. Phys.* **81**, 647–691 (2009).
84. P. Mason, N. Berloff, A. Fetter, Motion of a vortex line near the boundary of a semi-infinite uniform condensate. *Phys. Rev. A* **74**, 043611 (2006).
85. B. Anderson, P. Haljan, C. Wieman, E. Cornell, Vortex precession in Bose-Einstein condensates: Observations with filled and empty cores. *Phys. Rev. Lett.* **85**, 2857–2860 (2000).
86. D. Freilich, D. Bianchi, A. M. Kaufman, T. Langin, D. Hall, Real-time dynamics of single vortex lines and vortex dipoles in a Bose-Einstein condensate. *Science* **329**, 1182–1185 (2010).
87. E. Lundh, P. Ao, Hydrodynamic approach to vortex lifetimes in trapped Bose condensates. *Phys. Rev. A* **61**, 063612 (2000).
88. D. Sheehy, L. Radzihovsky, Vortices in spatially inhomogeneous superfluids. *Phys. Rev. A* **70**, 063620 (2004).
89. A. Svidzinsky, A. Fetter, Dynamics of a vortex in a trapped Bose-Einstein condensate. *Phys. Rev. A* **62**, 063617 (2000).